

Measurement of string tension and initial temperature from transverse momentum spectra of heavy quarkonia in proton-proton collisions at the LHC

Peng-Cheng Zhang^{1,*}, Hailong Zhu^{1,†}, Fu-Hu Liu^{1,‡}, Khusniddin K. Olimov^{2,3,§}

¹*Institute of Theoretical Physics & College of Physics and Electronic Engineering,*

State Key Laboratory of Quantum Optics Technologies and Devices &

Collaborative Innovation Center of Extreme Optics, Shanxi University, Taiyuan 030006, China

²*Laboratory of High Energy Physics, Physical-Technical Institute of Uzbekistan Academy of Sciences,*

Chingiz Aytmatov Str. 2b, Tashkent 100084, Uzbekistan

³*Department of Natural Sciences, National University of Science and Technology*

MISIS (NUST MISIS), Almalyk Branch, Almalyk 110105, Uzbekistan

Abstract: The string tension (κ) in the Schwinger mechanism and the effective temperature (T) in Bose-Einstein statistics are extracted from the transverse momentum (p_T) spectra of heavy quarkonia produced in proton-proton (p+p) collisions at the Large Hadron Collider (LHC). Here, T derived from the heavy quarkonium p_T spectra also represents the initial temperature of the collision system, as transverse flow has not yet formed when heavy quarkonia are produced. The related parameters (κ and T) are obtained by fitting the experimental p_T spectra of J/ψ and $\Upsilon(nS)$ ($n = 1, 2, \text{ and } 3$) within various rapidity intervals, produced in p+p collisions at center-of-mass energies of $\sqrt{s} = 13$ and 8 TeV, as measured by the LHCb Collaboration. It is found that the multi-component distribution structured within the framework of the Schwinger mechanism or Bose-Einstein statistics can effectively describe the heavy quarkonium p_T spectra in small collision systems. With decreasing rapidity in the forward region, both κ and T increase, indicating a directly proportional relationship between them. Based on κ , the average minimum strong force radius of participant quarks is determined.

Keywords: Schwinger mechanism; Bose-Einstein statistics; small collision system; string tension; initial temperature; linear relationship

PACS numbers: 12.40.Ee, 13.85.Hd, 13.85.Ni, 25.75.Ag, 25.75.Dw

I. INTRODUCTION

Current investigations reveal that small collision systems, such as proton-proton (p+p) or proton-nucleus collisions, also exhibit collectivity [1–4]. This phenomenon suggests that the temperature concept used in large collision systems, such as nucleus-nucleus collisions, can also be applied to small systems [5–7]. Generally, the final temperature of the collision system can be extracted from the yields or transverse momentum (p_T) spectra of identified light hadrons, which are produced in the thermal process and appear during the final kinetic freeze-out stage. In contrast, the initial temperature of the collision system can be extracted from the distribution properties of heavy quarkonia, which are produced at the initial stage [8–11]. Thus, temperatures extracted from the p_T spectra of different particles reflect the excitation degrees of the collision system at different stages.

* 202312602003@email.sxu.edu.cn

† Correspondence: zhuhl@sxu.edu.cn

‡ Correspondence: fuhuliu@163.com; fuhuliu@sxu.edu.cn

§ Correspondence: khkolimov@gmail.com; kh.olimov@uzsci.net

Typically, the temperature parameter used in p_T distributions refers to the so-called effective temperature (T), rather than the real thermal temperature, unless the influence of radial or transverse flow [12–15] is removed from the total amount. However, T extracted from the p_T spectra of heavy quarkonia may represent the real temperature because transverse flow does not form at the initial stage. In other words, if the p_T distribution with the parameter T in Bose-Einstein statistics is used to describe the production of heavy quarkonia [16–18], T indeed reflects the initial temperature. Although the initial temperature has received relatively little research attention in the community compared to the final temperature (chemical or kinetic freeze-out temperature), which has been extensively studied, it remains an important quantity for understanding the early dynamics of the collision system.

It is well understood that the mechanism of heavy quarkonium production in high-energy collisions involves the synergistic effects of perturbative and non-perturbative quantum chromodynamics (QCD) [19–21]. Despite heavy quarkonia not being purely produced via a thermal process, statistical results from a large number of events exhibit similar laws to thermal processes [22–25]. Therefore, the statistical laws applicable to thermal processes can also be applied to the production of heavy quarkonia. Due to differing interaction mechanisms, one might consider T from heavy quarkonium spectra as an extensive temperature. For consistency, however, we prefer to refer to T from heavy quarkonium spectra as the initial temperature in this work. This temperature perfectly reflects the statistical process and is unaffected by transverse flow.

Quantum statistics (Bose-Einstein and Fermi-Dirac) [26–28] have been widely applied in particle and nuclear physics, although classical (Boltzmann-Gibbs) statistics serve as a suitable approximation in most cases [29–31]. Of course, a single-component distribution from quantum statistics cannot adequately describe the p_T spectra. Instead, two- or multi-component distributions play a significant role. As products generated at the initial stage, the behavior characteristics of heavy quarkonia, such as J/ψ and $\Upsilon(nS)$ ($n = 1, 2, \text{ and } 3$), reflect the strength of initial interactions among participant partons. The multi-component distribution derived from Bose-Einstein statistics (or the multi-component Bose-Einstein distribution) can describe the p_T spectra of J/ψ and $\Upsilon(nS)$ and extract the initial temperature T of collision systems.

Alternatively, the Schwinger mechanism distribution (or Schwinger distribution) can be utilized to describe the interaction strength between two participant partons in high-energy collisions, albeit this application remains relatively uncommon [32–35]. Naturally, single-, two-, or multi-component Schwinger distributions can be employed depending on the specific scenarios. Compared with proton-nucleus and nucleus-nucleus collisions, p+p collisions exhibit particular advantages due to the minimal influence of spectator partons. Here, the participant-spectator model [36–39] widely used in proton-nucleus and nucleus-nucleus collisions is extended to p+p collisions, where participants and spectators are considered partons when studying heavy quarkonium production.

The Schwinger mechanism describes particle production at the parton level, while Bose-Einstein statistics characterizes the behavior of bosons. We aim to extract the string tension (κ) from the Schwinger mechanism [32–35] and the temperature T from Bose-Einstein statistics [29–31], subsequently investigating the relationship between κ and T . In this study, multi-component Schwinger and Bose-Einstein distributions are employed to describe the p_T spectra of J/ψ and $\Upsilon(nS)$ produced in p+p collisions at center-of-mass energies of $\sqrt{s} = 13$ and 8 TeV, as measured by the LHCb Collaboration at the Large Hadron Collider (LHC) [40–43]. The parameters κ and T are extracted, and their relationship is determined. Additionally, based on κ , the average minimum strong force radius is also obtained.

The remainder of this article is structured as follows: Section 2 outlines the formalism associated with the Schwinger mechanism and Bose-Einstein statistics. Results and discussions are presented in Section 3. Finally, Section 4 provides a summary and conclusions.

II. FORMALISM FROM SCHWINGER MECHANISM AND BOSE-EINSTEIN STATISTICS

Based on the Schwinger mechanism [32–35], a multi-component distribution can be formulated. Each component i arises from the contribution of two participant partons, where each parton j contributes transverse momentum (p_{tj})

via a Gaussian-type probability density function $f_{ij}(p_{tj})$. This is expressed as:

$$\begin{aligned} f_{ij}(p_{tj}) &= C_0(\kappa_i) \exp \left[-\frac{\pi(p_{tj}^2 + m_0^2)}{\kappa_i} \right] \\ &= C_0(\kappa_i) \exp \left(-\frac{\pi m_0^2}{\kappa_i} \right) \exp \left(-\frac{\pi p_{tj}^2}{\kappa_i} \right) \\ &= \frac{1}{\sqrt{\kappa_i}} \exp \left(-\frac{\pi p_{tj}^2}{\kappa_i} \right), \end{aligned} \quad (1)$$

where m_0 represents the rest mass of the participant parton, κ_i denotes the string tension, and $C_0(\kappa_i)$ is the normalization constant.

The final p_T of a particle in component i results from the contributions of two participant partons, following the folding of their individual contributions. The p_T distribution in component i is given by:

$$\begin{aligned} f_i(p_T) &= \int_0^{p_T} f_{i1}(p_{t1}) f_{i2}(p_T - p_{t1}) dp_{t1} \\ &= \int_0^{p_T} f_{i2}(p_{t2}) f_{i1}(p_T - p_{t2}) dp_{t2} \\ &= \frac{1}{\kappa_i} \int_0^{p_T} \exp \left\{ -\frac{\pi[p_{t1}^2 + (p_T - p_{t1})^2]}{\kappa_i} \right\} dp_{t1} \\ &= \frac{1}{\kappa_i} \int_0^{p_T} \exp \left\{ -\frac{\pi[p_{t2}^2 + (p_T - p_{t2})^2]}{\kappa_i} \right\} dp_{t2}, \end{aligned} \quad (2)$$

which is normalized to unity. Let k_i denote the fraction contributed by component i . The final p_T distribution from the multi-component system can then be written as:

$$f(p_T) = \sum_i k_i f_i(p_T), \quad (3)$$

with $\sum_i k_i = 1$ due to normalization. The average string tension weighted by k_i in the multi-component Schwinger distribution is $\kappa = \sum_i k_i \kappa_i$.

In terms of Bose-Einstein statistics [29–31], for component i with effective temperature T_i , the invariant yield or boson momentum (p) distribution is expressed as [29]:

$$E \frac{d^3 N_i}{d^3 p} = \frac{g V_i}{(2\pi)^3} E \left[\exp \left(\frac{E - \mu}{T_i} \right) - 1 \right]^{-1}, \quad (4)$$

where N_i is the number of bosons, $g = 1$ is the degeneracy factor for bosons, μ is the chemical potential (close to zero at high energy), $E = \sqrt{p^2 + m_0^2} = m_T \cosh y$ is the energy, m_0 is the rest mass, $m_T = \sqrt{p_T^2 + m_0^2}$ is the transverse mass, $y = (1/2) \ln[(E + p_z)/(E - p_z)]$ is the rapidity, p_z is the longitudinal momentum of the considered boson, and V_i is the volume of the collision system.

The probability density function of p_T in component i is:

$$\begin{aligned} f_i(p_T) &= \frac{1}{N_i} \frac{dN_i}{dp_T} \\ &= \frac{1}{N_i} \frac{g V_i}{(2\pi)^2} p_T \sqrt{p_T^2 + m_0^2} \int_{y_{\min}}^{y_{\max}} \cosh y \\ &\quad \times \left[\exp \left(\frac{\sqrt{p_T^2 + m_0^2} \cosh y - \mu}{T_i} \right) - 1 \right]^{-1} dy, \end{aligned} \quad (5)$$

where y_{\min} and y_{\max} are the minimum and maximum rapidities, respectively, within the experimental rapidity interval $[y_{\min}, y_{\max}]$. The multi-component distribution is expressed as:

$$f(p_T) = \frac{1}{N} \frac{dN}{dp_T} = \sum_i k_i \frac{1}{N_i} \frac{dN_i}{dp_T} = \sum_i k_i f_i(p_T), \quad (6)$$

which is consistent with Eq. (3). The average temperature from the multi-component Bose-Einstein distribution is given by $T = \sum_i k_i T_i$.

In the multi-component Schwinger (Bose-Einstein) distribution, the functional forms of various components remain consistent, despite differences in parameter values due to observed commonalities, similarities [44–47], and universality [48–51] in high-energy collisions. Variations in parameter values arise from differing strengths or degrees of analogous processes.

III. RESULTS AND DISCUSSION

Figure 1 illustrates the double differential cross section, $d^2\sigma/(dydp_T)$, of (a) prompt J/ψ and (b) J/ψ originating from b -quarks in p+p collisions at $\sqrt{s} = 13$ TeV, where σ denotes the cross section. Figure 2 depicts the double differential cross section, $d^2\sigma/(dydp_T)$, of (a) $\Upsilon(1S)$, (b) $\Upsilon(2S)$, and (c) $\Upsilon(3S)$ produced in p+p collisions at $\sqrt{s} = 13$ TeV. Similarly, Figure 3 displays the double differential cross section, $d^2\sigma/(dydp_T)$, of (a) prompt J/ψ and (b) J/ψ from b -quarks in p+p collisions at $\sqrt{s} = 8$ TeV, while Figure 4 presents the double differential cross section, $d^2\sigma/(dydp_T)$, of (a) $\Upsilon(1S)$, (b) $\Upsilon(2S)$, and (c) $\Upsilon(3S)$ produced in p+p collisions at $\sqrt{s} = 8$ TeV. In Figures 1–4, different symbols represent experimental data measured by the LHCb Collaboration in various y intervals within the forward rapidity region at the LHC [40–43]. Solid and dashed curves correspond to our results fitted using three-component Schwinger and Bose-Einstein distributions, respectively. To enhance clarity, experimental data and fitted results are rescaled by factors indicated in the panels. Using the least square method, optimal parameter values are obtained during fitting. It is evident that the experimental double differential cross sections of J/ψ and $\Upsilon(nS)$ across different y intervals in 13 and 8 TeV p+p collisions, as measured by the LHCb Collaboration, can be accurately described by three-component Schwinger and Bose-Einstein distributions.

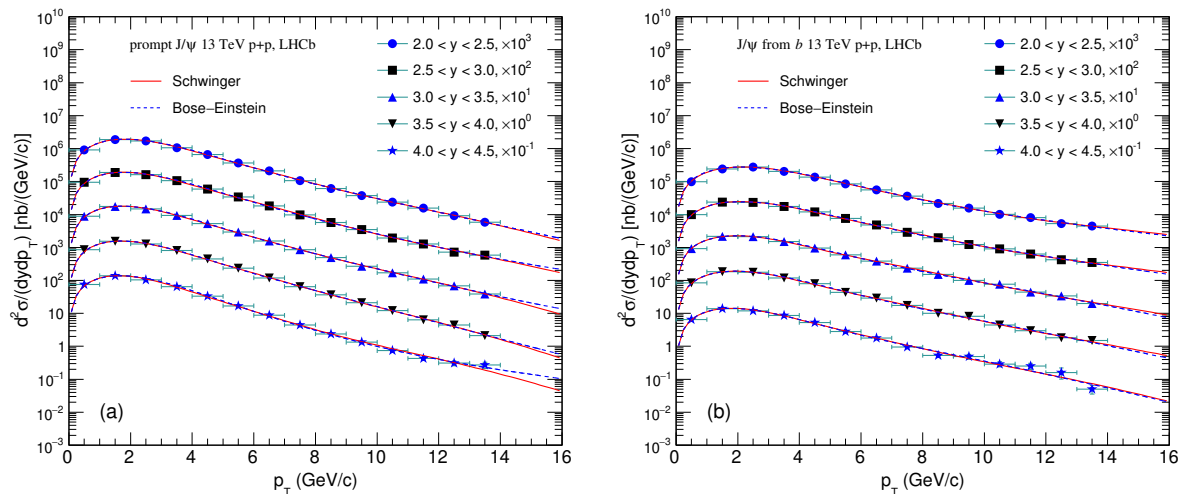


Figure 1. The double differential cross section, $d^2\sigma/(dydp_T)$, for (a) prompt J/ψ and (b) J/ψ from b produced in p+p collisions at $\sqrt{s} = 13$ TeV. Different symbols represent experimental data in various y intervals measured by the LHCb Collaboration [40], with the data rescaled by different factors for clarity. The solid and dashed curves correspond to our results fitted using three-component Schwinger and Bose-Einstein distributions, respectively.

To explore the relationship between κ and T , Figures 5(a) and 5(b) depict results derived from the spectra of heavy quarkonia J/ψ and $\Upsilon(nS)$ produced in p+p collisions at $\sqrt{s} = 13$ and 8 TeV, respectively. For each case — i) prompt J/ψ , ii) J/ψ from b , iii) $\Upsilon(1S)$, iv) $\Upsilon(2S)$, and v) $\Upsilon(3S)$ — the result corresponding to $2.0 < y < 2.5$ is positioned at the higher edge, whereas the result for $4.0 < y < 4.5$ is located at the lower edge. Values gradually increase from

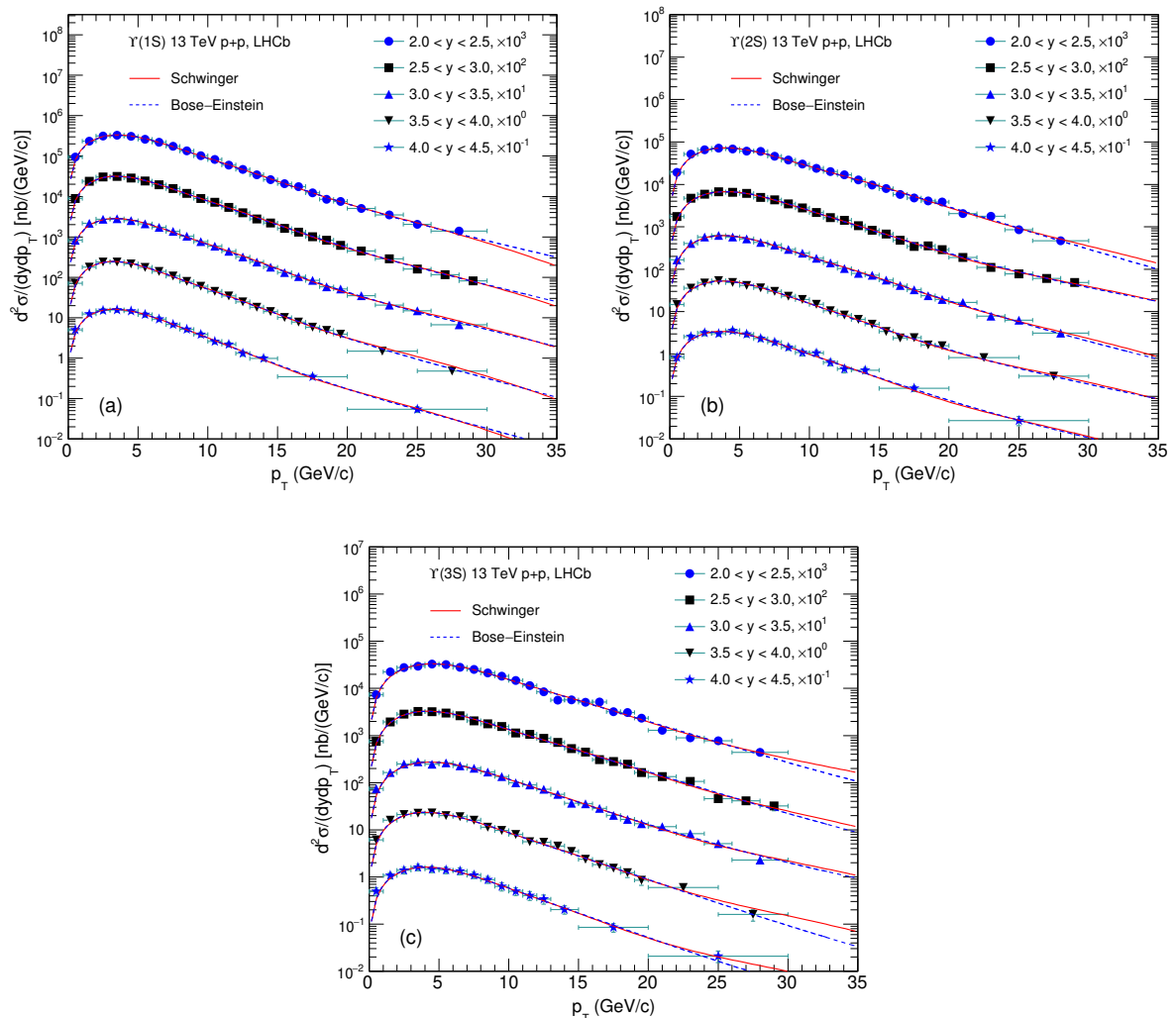


Figure 2. The double differential cross section, $d^2\sigma/(dydp_T)$, for (a) $\Upsilon(1S)$, (b) $\Upsilon(2S)$, and (c) $\Upsilon(3S)$ produced in p+p collisions at $\sqrt{s} = 13$ TeV. Different symbols represent experimental data in various y intervals measured by the LHCb Collaboration [41], with the data rescaled by different factors for clarity. The solid and dashed curves correspond to our results fitted using three-component Schwinger and Bose-Einstein distributions, respectively.

$4.0 < y < 4.5$ to $2.0 < y < 2.5$. It is observed that the relationship between κ and T is approximately linear for each case. However, considering all five cases collectively, the relationship between κ and T exhibits complexity.

The values of κ and T extracted from the spectra of prompt J/ψ , J/ψ from b , $\Upsilon(1S)$, $\Upsilon(2S)$, and $\Upsilon(3S)$ increase in an orderly manner. This reflects the interaction strength between two participant partons as well as the magnitude of the average transverse momenta of the bosons themselves. Given the initial temperature (~ 0.75 – 2.15 GeV at $\sqrt{s} = 13$ TeV and ~ 0.69 – 1.98 GeV at $\sqrt{s} = 8$ TeV), T is significantly larger than the chemical freeze-out temperature (~ 0.16 GeV) determined by the statistical (thermal) model and hydrodynamical description [52–55] and the kinetic freeze-out temperature (~ 0.10 – 0.16 GeV) derived from the blast wave model [56–59]. While this relative size appears to be a natural outcome, direct comparisons among the three temperatures are not feasible due to their differing definitions.

Although the initial temperatures extracted by us are significantly higher than typical QGP freeze-out temperatures (~ 0.16 GeV), our results are comparable to those obtained using the color string percolation method [60–62], which was employed in our previous work [63–65]; the relative fugacities of quarks and gluons method [66]; a comprehensive heavy ion model evaluation and reporting algorithm [67]; and a perfect relativistic hydrodynamic solution based on direct photon observables [68–71]. The present results are lower than those from the color string percolation method

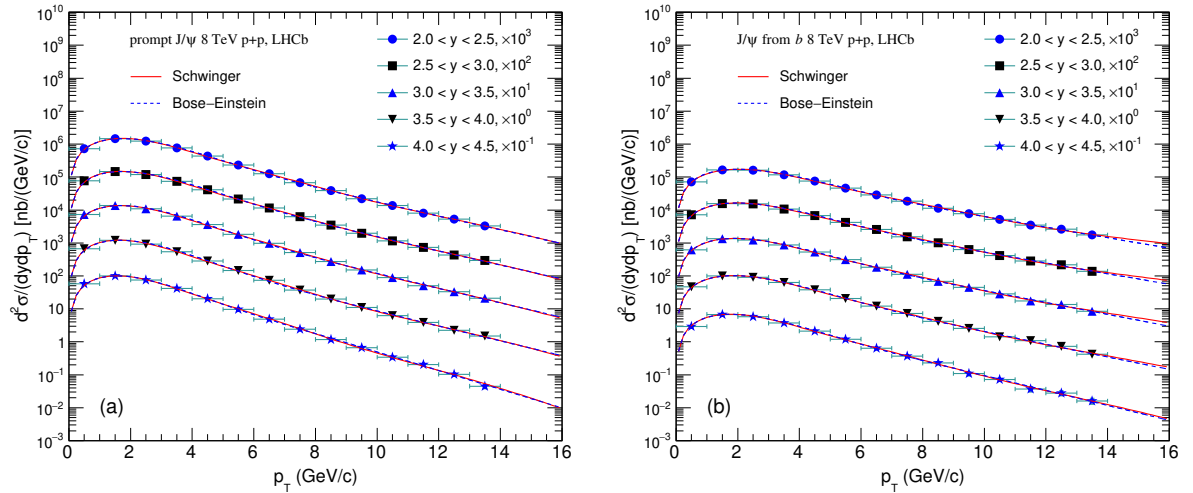


Figure 3. The double differential cross section, $d^2\sigma/(dydp_T)$, for (a) prompt J/ψ and (b) J/ψ from b produced in p+p collisions at $\sqrt{s} = 8$ TeV. Different symbols represent experimental data in various y intervals measured by the LHCb Collaboration [42], with the data rescaled by different factors for clarity. The solid and dashed curves correspond to our results fitted using three-component Schwinger and Bose-Einstein distributions, respectively.

(~ 2.5 – 6.5 GeV) [63] at the same energy but higher than those from the relative fugacity method (~ 0.2 – 0.6 GeV at $\sqrt{s_{NN}} = 200$ – 5020 GeV) [66], the comprehensive algorithm (~ 0.3 – 0.4 GeV at $\sqrt{s_{NN}} = 200$ GeV) [67], and the perfect hydrodynamic solution (~ 0.4 – 0.5 GeV at $\sqrt{s_{NN}} = 200$ GeV) [68–71], although some of these methods focus on lower collision energies.

If the definitions of initial, chemical freeze-out, and kinetic freeze-out temperatures are consistent and well-coordinated, a direct comparison among them becomes feasible. As the collision system evolves over time, its temperature gradually decreases. Typically, the initial temperature is higher than the chemical freeze-out temperature, which in turn is higher than the kinetic freeze-out temperature. In certain cases, if chemical and kinetic freeze-outs occur simultaneously, the chemical freeze-out temperature may equal the kinetic freeze-out temperature.

To understand how the parameters κ and T depend on the collision energy \sqrt{s} , we have conducted an estimation. It is known that κ and T are primarily determined by the energy density of the collision system. According to lattice QCD calculations [72], the energy density is proportional to the fourth power of the temperature, and it increases with increasing \sqrt{s} . Consequently, both κ and T exhibit a nonlinear growth trend as \sqrt{s} increases. At $\sqrt{s} = 13$ and 8 TeV discussed in this work, the ratio of the parameters at different energies aligns more closely with $\ln(13000)/\ln(8000)$ than with $13000/8000$ or $\sqrt{13000/8000}$, where \sqrt{s} is expressed in GeV to ensure parameter consistency. This suggests a potential relationship: $\kappa = a_1 + b_1 \ln \sqrt{s}$ or $T = a_2 + b_2 \ln \sqrt{s}$, where $a_{1,2}$ and $b_{1,2}$ represent the intercept and slope coefficients, respectively. Determining the precise dependence of these parameters on collision energy requires further data fitting across various energies in future.

Based on κ , the average minimum distance between the two participant quarks [$c\bar{c}$ for J/ψ or $b\bar{b}$ for $\Upsilon(nS)$] can be calculated. According to the Schwinger mechanism [32–35], the average minimum distance is given by $2m_0/\kappa$. This distance also corresponds to twice the average minimum radius R_{\min} of the strong interaction force between the two quarks, where $R_{\min} = m_0/\kappa$. The dependence of R_{\min} on y , extracted from the spectra of heavy quarkonia produced in p+p collisions at $\sqrt{s} = 13$ and 8 TeV, is illustrated in Figures 6(a) and 6(b), respectively. It is evident that R_{\min} decreases as y decreases from $4.0 < y < 4.5$ to $2.0 < y < 2.5$ in the forward rapidity region. Extremely small values of R_{\min} ($0.03 \sim 0.09$ fm) are obtained, which are one tenth of various radii (hard-core, charge, mass, axial) of nucleons ($0.3 \sim 1.0$ fm) [73–75].

We would like to emphasize that the minimum strong force radii (Figure 6) of c and b quarks are significantly smaller than the sizes (~ 0.4 and ~ 0.2 fm) of different quarkonia [J/ψ and $\Upsilon(nS)$] obtained via the potential model [76–79].

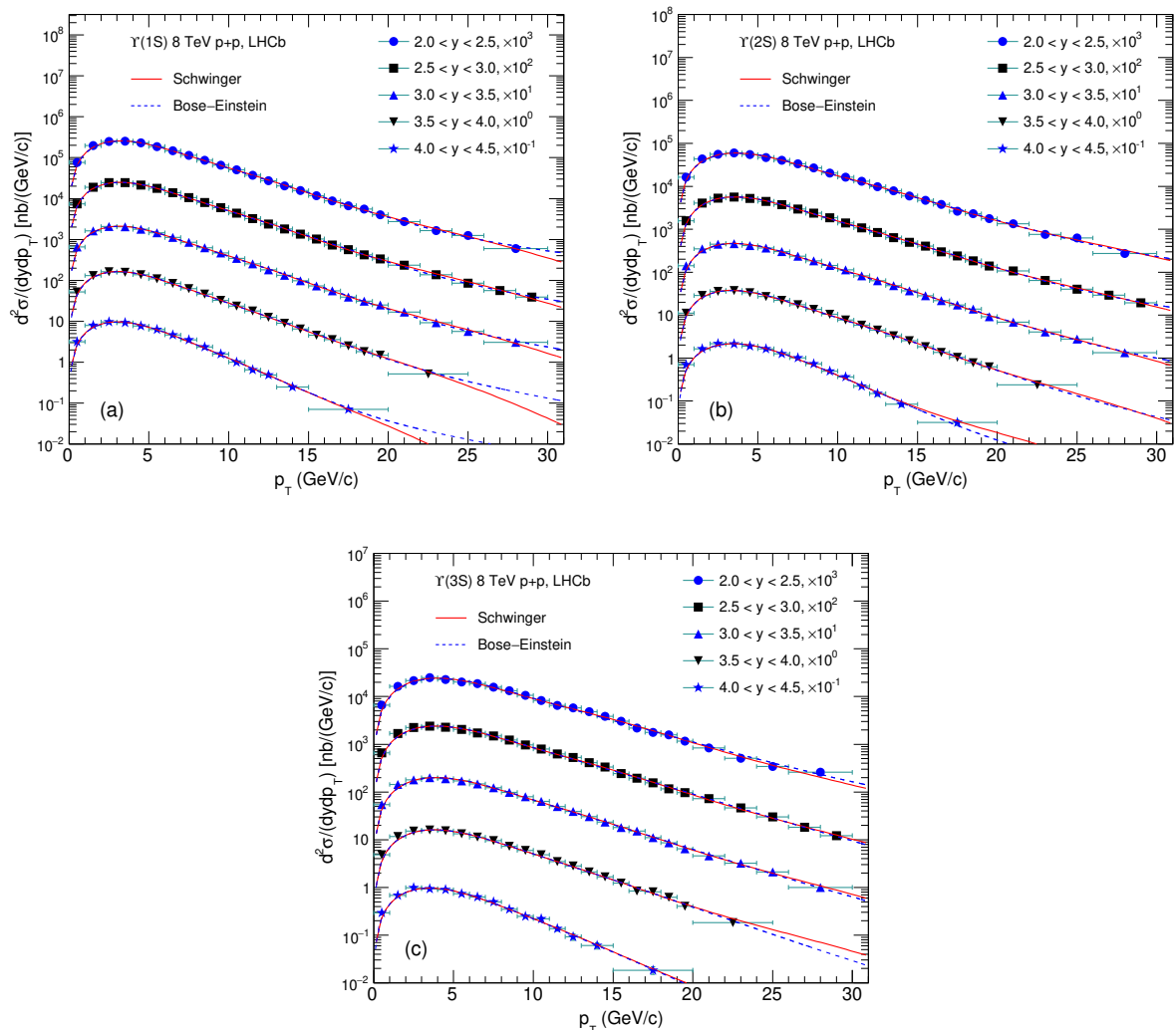


Figure 4. The double differential cross section, $d^2\sigma/(dydp_T)$, for (a) $\Upsilon(1S)$, (b) $\Upsilon(2S)$, and (c) $\Upsilon(3S)$ produced in p+p collisions at $\sqrt{s} = 8$ TeV. Different symbols represent experimental data in various y intervals measured by the LHCb Collaboration [43], with the data rescaled by different factors for clarity. The solid and dashed curves correspond to our results fitted using three-component Schwinger and Bose-Einstein distributions, respectively.

This indicates that c and b quarks are extremely close when forming quarkonia. Nevertheless, within quarkonia, c and b quarks still possess sufficient space for movement. This situation resembles that of quarks inside nucleons, where quarks are much smaller than the nucleons themselves. The radius of quarkonium is typically calculated based on its form factor or decay parameters, including lattice QCD, QCD sum rules, and related data analyses. The analysis of the minimum strong force radius R_{\min} of heavy quarks presented in this article provides an indirect measurement derived from the transverse momentum spectra of quarkonia, although R_{\min} does not directly correspond to the size of quarkonia.

The value of R_{\min} is approximately an order of magnitude smaller than nucleon radii. Such a small radius is physically plausible for quark-antiquark binding at the LHC. Due to the extremely high collision energy, the colliding protons undergo significant mutual compression, penetration, and overlap, bringing the quark and antiquark that constitute quarkonium into very close proximity—potentially even closer than the proton radius. It is anticipated that at higher collision energies, the value of R_{\min} will decrease further. Conversely, at lower collision energies, R_{\min} will increase. If the collision energy is sufficiently low while still allowing for quarkonium production, R_{\min} could exceed the proton radius or even be several times larger than it.

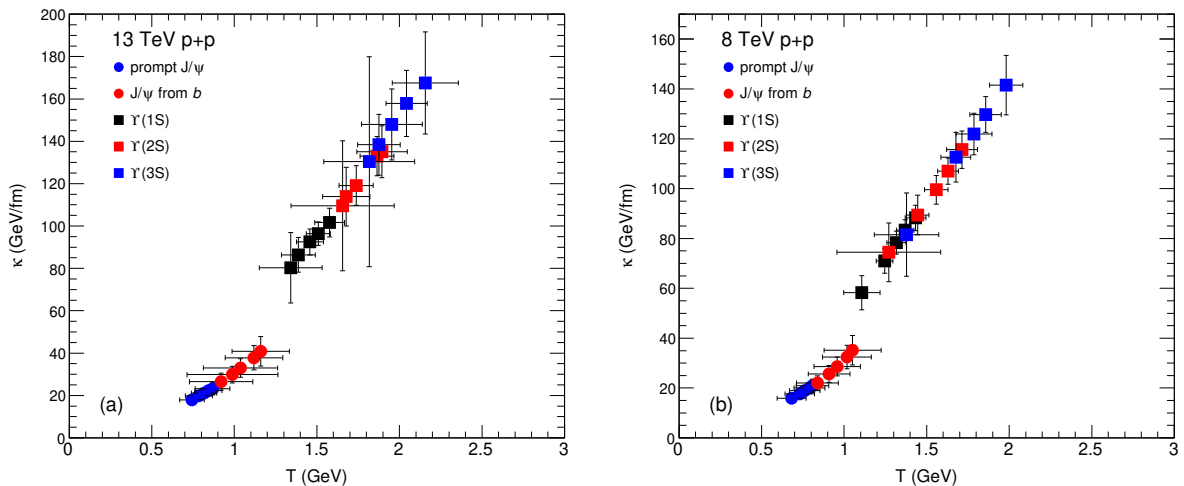


Figure 5. Relationship between string tension κ and initial temperature T derived from the spectra of heavy quarkonia J/ψ and $\Upsilon(nS)$ produced in p+p collisions at (a) 13 TeV and (b) 8 TeV. Results corresponding to $2.0 < y < 2.5$ ($4.0 < y < 4.5$) are located at the higher (lower) value edge for each case. Five cases are illustrated in the panels.

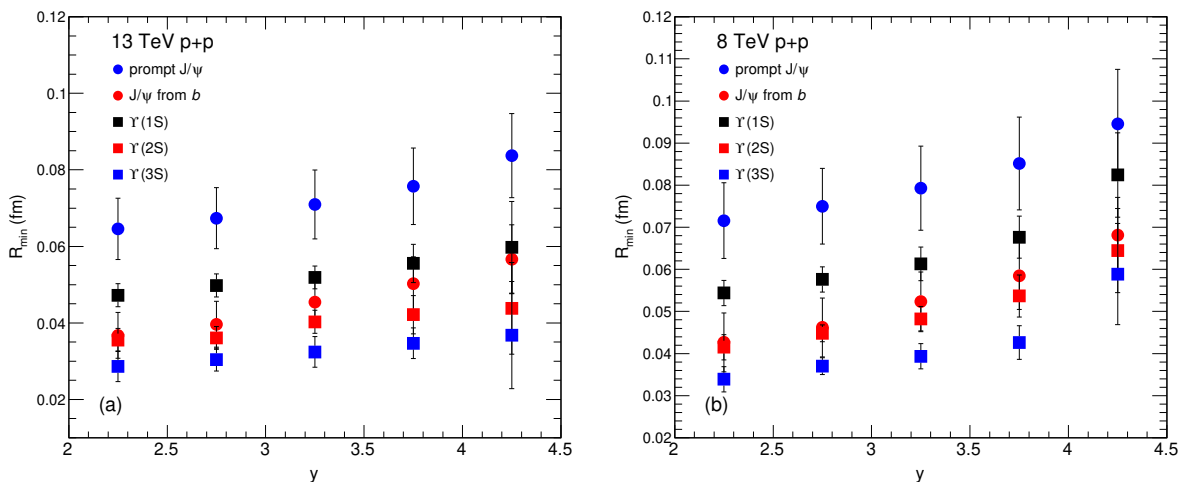


Figure 6. Dependence of the average minimum strong force radius R_{\min} of participant c or b quarks on the rapidity y of quarkonium extracted from p+p collisions at (a) 13 TeV and (b) 8 TeV. Five cases are illustrated in the panels.

The dependence of quarkonium production on charged-particle multiplicity has been extensively studied both experimentally and theoretically [80–83]. These studies reveal diverse trends. In general, in high-energy p+p collisions, where conditions for QGP formation are absent, the quarkonium yield is mainly influenced by the distribution of initial-state partons and the final-state hadronization process, with a relatively linear relationship to the multiplicity of charged particles. In contrast, in high-energy heavy ion collisions, as the multiplicity increases, the QGP effect becomes more pronounced, leading to a nonlinear suppression of quarkonium yield—such as the “sequential suppression” phenomenon observed in $\Upsilon(nS)$ and J/ψ . Heavier collision systems exhibit more significant suppression. The present work does not investigate the parameter dependence on charged-particle multiplicity but instead focuses on quarkonium rapidity, due to differing research objectives.

Comparing relevant parameters across different distributions holds great significance in high-energy collisions. In our previous and recent studies [84–88], we have investigated the parameters associated with string tension, effective temperature, and average transverse momentum extracted from the transverse momentum spectra of particles

produced in both large and small collision systems. Approximate linear correlations under specific restrictive conditions have been identified. The present work further validates these observations by comparing the string tension in the Schwinger mechanism with the effective temperature in Bose-Einstein statistics in p+p collisions at the LHC. This study provides an important perspective for researchers to deepen their understanding of system evolution and interaction mechanisms.

The string tension characterizes the energy density per unit length of the color flux tube in QCD, representing the gradient of quark confinement strength and the strong interaction potential. Its numerical value directly influences the critical energy threshold for string breaking during hadronization and determines the transverse momentum distribution of particles. The effective temperature reflects the degree of thermalization in high-temperature and high-density systems and is directly linked to transport properties such as sound velocity and viscosity coefficients. Larger values result in a broader transverse momentum distribution of particles.

The experimental determination of string tension can verify the consistency between the QCD string model and lattice calculation predictions, providing a benchmark for describing strong interactions beyond perturbation theory. Simultaneously, when coupled with non-equilibrium dynamics, string tension may induce the formation of strange hadron states (e.g., color superconducting states). Abnormal fluctuations in the effective temperature may indicate the critical region in the QCD phase diagram, verifying the phase transition paths predicted by lattice QCD. Furthermore, the correlation between the effective temperature and boson occupancy can reveal collective excitations dominated by boson modes during the quark-gluon plasma (QGP) de-confinement process.

In the extraction of string tension, there exists a challenge regarding insufficient real-time detection accuracy in non-perturbative processes. Future research could focus on developing case reconstruction algorithms based on deep learning to address this issue. Similarly, in the extraction of effective temperature, measurement model distortion caused by multi-body correlation effects poses a significant problem. This can potentially be resolved by constructing thermodynamic evolution equations that incorporate quantum entanglement. As these are fundamental research tasks, accurately extracting their values is essential for meaningful comparisons and understanding their relationships.

Based on the aforementioned discussion, it can be inferred that through synergistic analysis of string tension and effective temperature, researchers can reconstruct the collision dynamics of the complete spatiotemporal chain, from the initial energy deposition of the color field to the evolution of the thermalization medium. This approach allows for comparing prediction differences between the string model and the thermal/statistical model for the same observation, enabling cross-validation of the models. Furthermore, it explores the possibility of discovering strong interaction corrections or Bose condensation phases beyond the standard model in the TeV energy region. In short, the cross-study of these two parameters provides a unique perspective for uncovering the deep structure of matter and the early evolution laws of the universe.

It should be noted that numerous studies have explored light and heavy flavor production using the Schwinger mechanism combined with fluctuations in string tension [89, 90]. Compared to the high p_T production of light quarks (u , d , and s), the production of heavy quarks (c and b) shows less suppression, which is attributed to the dead cone effect [91–93]. The experimental data cited in this work exhibit a long-tail distribution, reflecting reduced suppression at high p_T , which is associated with the dead cone effect. Generally, heavy quarks exhibit a more pronounced dead cone effect due to their large mass. Gluons, being massless, do not exhibit such an effect, and the dead cone effect for light quarks is negligible due to their small mass.

Moreover, if the fluctuations in string tension follow a Gaussian distribution, they can lead to thermal production characterized by exponential p_T distributions. If the fluctuations follow a Tsallis-type distribution, they result in thermal production at low p_T and power-law behavior at high p_T [94, 95]. In most cases, the observed data align better with a combination of thermal production at low p_T and power-like production at high p_T . This distinction across p_T regions implies different underlying interaction mechanisms or degrees of excitation. The present work employs the same functional form with varying parameters for different p_T ranges, indicating a multi-component distribution and resulting in temperature fluctuations. These temperature fluctuations reflect variations in string tension, highlighting the intrinsic connection between temperature and string tension.

Before summarizing and concluding, we would like to emphasize recent observations of collective effects in small systems at the LHC [96, 97], which suggest transient thermalization. Additionally, the LHCb experimental data used in our analysis represent high-statistics results. Our application of the Bose-Einstein distribution serves solely as a statistical tool to characterize spectral features and extract temperature parameters or average kinetic energies across many events. We do not claim thermal equilibrium—only high statistical reliability. Furthermore, apart from heavy quarkonium production, a vast majority of particles produced in high-energy collisions contain light quarks. It is estimated that pions account for approximately 80–90% of the total hadron yield, while heavy quarkonia contribute less than 1% [40–43], with the remaining fraction distributed among various other particles. Typically, particles with larger masses constitute smaller proportions.

Although heavy quarks are indeed produced through hard processes, our focus lies in their hadronization outcomes, where non-perturbative effects—such as string fragmentation—dominate. Rather than pursuing detailed micro-processes, we treat our methods as statistical tools to extract meaningful quantities that may serve as references for future studies. If heavy quarks (c and b) produced via perturbative QCD—such as those predicted by Fixed Order Next-to-Leading Log (FONLL) calculations [98, 99]—are considered within a microscopic framework, the present work focuses on the macroscopic statistical behavior of heavy quarkonia. Specifically, using simple analytical expressions, we perform an indirect estimation of the string tension. Although the extracted value appears unusually large, it may be refined through further calibration.

As is known [87, 88], classical and quantum statistics [26–31] yield higher temperature estimates compared to Tsallis statistics [100–104], which in turn yields higher values than q-dual statistics [104]. To unify these different temperature measures, one can systematically compare them and investigate the relationships among various models. Just as the temperature parameter is model-dependent, it is possible that the string tension is also model-dependent. To reconcile the string tension used in the Schwinger mechanism [32–35] with that in PYTHIA and other microscopic models [105–108], one may consider reducing the amplitude of the string tension in the Schwinger mechanism through an appropriate correction method, such as scaling it down by a factor of 1/100 or taking the square root of its original value. The exact functional form or the relationship between string tensions in the Schwinger mechanism and other models needs to be determined through systematic comparisons in future studies.

According to our comparative analysis, the most plausible explanation is that the string tension used in the Schwinger mechanism primarily reflects the interaction strength at the initial stage of high-energy collisions. In fact, this string tension serves as an effective measure of the initial-stage temperature. Unlike dynamic models, there is no time evolution associated with the Schwinger string, since its tension is extracted based on static transverse momentum spectra of specific particles. This represents a fundamental difference from the string tension used in the Cornell potential and that obtained from finite-temperature lattice QCD simulations [109, 110]. If the Schwinger mechanism is applied to the spectra of various particles—each produced at different stages of the collision—it may be possible to extract a time-evolving picture of the string tension. This will be one of the key focuses of our future research.

IV. SUMMARY AND CONCLUSIONS

The transverse momentum spectra (double differential cross sections) of J/ψ and $\Upsilon(nS)$ produced in p+p collisions at $\sqrt{s} = 13$ and 8 TeV within different rapidity intervals are analyzed using the Schwinger mechanism and Bose-Einstein statistics. The multi-component distribution successfully fits the experimental results measured by the LHCb Collaboration. Our study demonstrates that both the string tension and initial temperature increase as rapidity decreases in the forward rapidity region, indicating a positive correlation between these parameters.

At higher collision energies, the string tension and initial temperature correspond to larger values, reflecting greater deposited energy in the collisions. For the production of i) prompt J/ψ , ii) J/ψ from b , iii) $\Upsilon(1S)$, iv) $\Upsilon(2S)$, and v) $\Upsilon(3S)$, both parameters increase sequentially. This suggests that more collision energy is required

for $\Upsilon(nS)$ production due to the larger mass of participating quarks ($b\bar{b}$). Based on the Schwinger mechanism, the minimum strong force radii of c and b quarks in the formation of J/ψ and $\Upsilon(nS)$ are approximately $0.03 \sim 0.09$ fm.

Author Contributions: The authors contributed to the paper in this way: conceptualization, H.L.Z., F.H.L. and K.K.O.; methodology, H.L.Z., F.H.L. and K.K.O.; software, P.C.Z.; validation, H.L.Z., F.H.L. and K.K.O.; formal analysis, P.C.Z.; investigation, P.C.Z.; resources, P.C.Z.; data curation, P.C.Z.; writing—original draft preparation, P.C.Z.; writing—review and editing, H.L.Z., F.H.L. and K.K.O.; visualization, P.C.Z.; supervision, H.L.Z., F.H.L. and K.K.O.; project administration, H.L.Z. and F.H.L.; funding acquisition, H.L.Z., F.H.L. and K.K.O. All authors have read and agreed to the published version of the manuscript.

Funding: The work of Shanxi group was supported by National Natural Science Foundation of China under Grant No. 12147215, Fundamental Research Program of Shanxi Province under Grant No. 202303021221071, Shanxi Scholarship Council of China and the Fund for Shanxi “1331 Project” Key Subjects Construction. The work of K.K.O. was supported by the Ministry of Innovative Development of the Republic of Uzbekistan within the fundamental project No. F3-20200929146 on analysis of open data on heavy-ion collisions at RHIC and LHC.

Data Availability Statement: The data used to support the findings of this study are included within the article and are cited at relevant places within the text as references.

Conflicts of Interest: The authors declare that there are no conflicts of interest regarding the publication of this paper. The funders had no role in the design of the study; in the collection, analysis, or interpretation of the data; in the writing of the manuscript; or in the decision to publish the results.

-
- [1] Guo, S.; Wang, H.S.; Zhou, K.; Ma, G.L. Machine learning study to identify collective flow in small and large colliding systems. *Phys. Rev. C* **2024**, *110*, 024910.
 - [2] Bhalerao, R.S. Collectivity in large and small systems formed in ultrarelativistic collisions. *Eur. Phys. J. Spec. Top.* **2021**, *230*, 635–654.
 - [3] Lacey, R.A. [for the STAR Collaboration]. Long-range collectivity in small collision-systems with two- and four-particle correlations @ STAR. *Nucl. Phys. A* **2021**, *1005*, 122041.
 - [4] Schlichting, S.; Tribedy, P. Collectivity in small collision systems: an initial-state perspective. *Adv. High Energy Phys.* **2016**, *2016*, 8460349.
 - [5] Biró, T.S. *Is there a temperature? conceptual challenges at high energy, acceleration and complexity*; Springer New York; New York, USA, 2011.
 - [6] Badshah, M.; Waqas, M.; Khubrani, A.M.; Ajaz, M. Systematic analysis of the pp collisions at LHC energies with Tsallis function. *Europhys. Lett.* **2023**, *141*, 64002.
 - [7] Waqas, M.; Peng, G.X.; Ajaz, M.; Ismail, A.H.; Wazir, Z.; Li, L.L. Extraction of different temperatures and kinetic freeze-out volume in high energy collisions. *J. Phys. G* **2022**, *49*, 095102.
 - [8] Lofnes, I.M. [for the ALICE Collaboration]. Quarkonia as probes of the QGP and the initial stages of the heavy-ion collisions with ALICE. *EPJ Web Conf.* **2022**, *259*, 12004.
 - [9] Wolschin, G. Aspects of relativistic heavy-ion collisions. *Universe* **2020**, *6*, 61.
 - [10] Song, T.; Ko, C.M.; Lee, S.H. Quarkonium formation time in relativistic heavy-ion collisions. *Phys. Rev. C* **2015**, *91*, 044909.
 - [11] Khan, P. [for the ALICE Collaboration]. Upsilon production in Pb-Pb and p-Pb collisions at forward rapidity with ALICE at the LHC. *J. Phys.: Conf. Ser.* **2014**, *509*, 012112.

- [12] Pandey, S.; Tiwari, S.K.; Singh, B.K. Pseudorapidity density, transverse momentum spectra, and elliptic flow studies in Xe-Xe collision systems at $\sqrt{s_{NN}} = 5.44$ TeV using the HYDJET++ model. *Phys. Rev. C* **2021**, *103*, 014903.
- [13] Nayak, S.R.; Pandey, S.; Singh, B.K. Beam energy dependence of transverse momentum distribution and elliptic flow in Au-Au collisions using HYDJET++ model. *Eur. Phys. J. Plus* **2025**, *140*, 375.
- [14] Badshah, M.; Ajaz, M.; Waqas, M.; Younis, H. Evolution of effective temperature, kinetic freeze-out temperature and transverse flow velocity in pp collision. *Phys. Scr.* **2023**, *98*, 115306.
- [15] Radhakrishnan, A.M.K.; Prasad, S.; Tripathy, S.; Mallick, N.; Sahoo, R. Investigating radial flow-like effects via pseudorapidity and transverse sphericity dependence of particle production in pp collisions at the LHC. *Eur. Phys. J. Plus* **2025**, *140*, 110.
- [16] Hong, J.; Lee, S.H. Energy loss of heavy quarkonia in hot QCD plasmas. *Phys. Rev. C* **2021**, *103*, 054907.
- [17] Durham, J.M. [for the PHENIX Collaboration]. Recent quarkonia studies from the PHENIX experiment. *Nucl. Phys. A* **2019**, *982*, 719–722.
- [18] Krouppa, B.; Rothkopf, A.; Strickland, M. Bottomonium suppression at RHIC and LHC. *Nucl. Phys. A* **2019**, *982*, 727–730.
- [19] Sharma, R.; Vitev, I. High transverse momentum quarkonium production and dissociation in heavy ion collisions. *Phys. Rev. C* **2013**, *87*, 044905.
- [20] Shifman, M. Persistent challenges of quantum chromodynamics. *Int. J. Mod. Phys. A* **2006**, *21*, 5695–5720.
- [21] Mocsy, A.; Petreczky, P.; Strickland, M. Quarkonia in the quark gluon plasma. *Int. J. Mod. Phys. A* **2013**, *28*, 1340012.
- [22] Bala, D.; Ali, S.; Kaczmarek, O.; Pavan; HotQCD Collaboration. Finite temperature quarkonia spectral functions in the pseudoscalar channel, J. Subat. Part. Cosmol. **2025**, *3*, 100042.
- [23] Vairo, A. Quarkonium dissociation in a thermal bath. *AIP Conf. Proc.* **2016**, *1701*, 020017.
- [24] Fadafan, K.B.; Tabatabaei, S.K. Thermal width of quarkonium from holography. *Eur. Phys. J. C* **2014**, *74*, 2842.
- [25] Brambilla, N.; Escobedo, M.A.; Ghiglieri, J.; Vairo, A. Thermal width and quarkonium dissociation by inelastic parton scattering. *J. High Energy Phys.* **2013**, *2013(05)*, 130.
- [26] Kolokoltsov, V.N. On a probabilistic derivation of the basic particle statistics (Bose-Einstein, Fermi-Dirac, canonical, grand-canonical, intermediate) and related distributions. *Trans. Mosc. Math. Soc.* **2021**, *82*, 93–104.
- [27] Dai, W.S.; Xie, M. Do bosons obey Bose-Einstein distribution: two iterated limits of Gentile distribution. *Phys. Lett. A* **2009**, *373*, 1524–1526.
- [28] Hasegawa, H. Bose-Einstein and Fermi-Dirac distributions in nonextensive quantum statistics: exact and interpolation approaches. *Phys. Rev. E* **2009**, *80*, 011126.
- [29] Cleymans, J.; D. Worku, D. Relativistic thermodynamics: transverse momentum distributions in high-energy physics. *Eur. Phys. J. A* **2012**, *48*, 160.
- [30] Gupta, R.; Jena, S. Model comparison of the transverse momentum spectra of charged hadrons produced in PbPb collision at $\sqrt{s_{NN}} = 5.02$ TeV. *Adv. High Energy Phys.* **2022**, *2022*, 5482034.
- [31] Jaiswal, A.; Roy, V. Relativistic hydrodynamics in heavy-ion collisions: general aspects and recent developments. *Adv. High Energy Phys.* **2016**, *2016*, 9623034.
- [32] Schwinger, J. On gauge invariance and vacuum polarization. *Phys. Rev.* **1951**, *82*, 664–679.
- [33] Wang, R.C.; Wong, C.Y. Finite-size effect in the Schwinger particle-production mechanism. *Phys. Rev. D* **1988**, *38*, 348–359.
- [34] Braun-Munzinger, P.; Redlich, K.; Stachel, J. Particle production in heavy ion collisions, in: *Quark-Gluon Plasma 3* (Eds: Hwa R.C.; Wang, X.N.); World Scientific; Singapore, 2004.
- [35] Wong, C.Y. *Introduction to High Energy Heavy Ion Collisions*; World Scientific; Singapore, 1994.
- [36] Glauber, R.L. in: *Lectures in Theoretical Physics* (Eds: Brittin, W.E.; Dunham L.G.); Interscience; New York, USA, 1959.
- [37] Shi, L.; Danielewicz, P.; Lacey, R. Spectator response to the participant blast. *Phys. Rev. C* **2001**, *64*, 034601.
- [38] Gaitanos, T.; Wolter, H.H.; Fuchs, C. Spectator and participant decay in heavy ion collisions. *Phys. Lett. B* **2000**, *478*, 79–85.

- [39] Sood, A.D; Puri, R.K. The study of participant-spectator matter and collision dynamics in heavy-ion collisions. *Int. J. Mod. Phys. E* **2006**, *15*, 899–910.
- [40] Aaij, R. et al. [LHCb collaboration]. Measurement of forward J/ψ production cross-sections in pp collisions at $\sqrt{s} = 13$ TeV. *J. High Energy Phys.* **2015**, *2015(10)*, 172.
- [41] Aaij, R. et al. [LHCb collaboration]. Measurement of Υ production in pp collisions at $\sqrt{s} = 13$ TeV. *J. High Energy Phys.* **2018**, *2018(07)*, 134.
- [42] Aaij, R. et al. [LHCb collaboration]. Production of J/ψ and Υ mesons in pp collisions at $\sqrt{s} = 8$ TeV. *J. High Energy Phys.* **2013**, *2013(06)*, 064.
- [43] Aaij, R. et al. [LHCb collaboration]. Forward production of Υ mesons in pp collisions at $\sqrt{s} = 7$ and 8 TeV. *J. High Energy Phys.* **2015**, *2015(11)*, 103.
- [44] Mishra, A.N.; Ortiz, A.; Paic, G. Intriguing similarities of high- p_T particle production between pp and A - A collisions. *Phys. Rev. C* **2019**, *99*, 034911.
- [45] Sarkisyan, E.K.G.; Sakharov, A.S. Multihadron production features in different reactions. *AIP Conf. Proc.* **2006**, *828*, 35–41.
- [46] Mishra, A.N.; Sahoo, R.; Sarkisyan, E.K.G.; Sakharov, A.S. Effective-energy budget in multiparticle production in nuclear collisions. *Eur. Phys. J. C* **2014**, *74*, 3147 and Erratum. *Eur. Phys. J. C* **2015**, *75*, 70.
- [47] Sarkisyan, E.K.G.; Sakharov, A.S. Relating multihadron production in hadronic and nuclear collisions. *Eur. Phys. J. C* **2010**, *70*, 533–541.
- [48] Sarkisyan, E.K.G.; Mishra, A.N.; Sahoo, R.; Sakharov, A.S. Multihadron production dynamics exploring the energy balance in hadronic and nuclear collisions. *Phys. Rev. D* **2016**, *93*, 054046 and Erratum. *Phys. Rev. D* **2016**, *93*, 079904.
- [49] Sarkisyan, E.K.G.; Mishra, A.N.; Sahoo, R.; Sakharov, A.S. Centrality dependence of midrapidity density from GeV to TeV heavy-ion collisions in the effective-energy universality picture of hadroproduction. *Phys. Rev. D* **2016**, *94*, 011501(R).
- [50] Sarkisyan, E.K.G.; Mishra, A.N.; Sahoo, R.; Sakharov, A.S. Effective-energy universality approach describing total multiplicity centrality dependence in heavy-ion collisions. *Europhys. Lett.* **2019**, *127*, 62001.
- [51] Castorina, P.; Iorio, A.; Lanteri, D.; Satz, H.; Spousta, M. Universality in hadronic and nuclear collisions at high energy. *Phys. Rev. C* **2020**, *101*, 054902.
- [52] Braun-Munzinger, P.; Stachel, J.; Wetterich, C. Chemical freeze-out and the QCD phase transition temperature. *Phys. Lett. B* **2004**, *596*, 61–69.
- [53] Andronic, A.; Braun-Munzinger, P.; Redlich, K.; Stachel, J. Decoding the phase structure of QCD via particle production at high energy. *Nature* **2018**, *561*, 321–330.
- [54] Flor, F.A.; Olinger, G.; Bellwied, R. Flavour and energy dependence of chemical freeze-out temperatures in relativistic heavy ion collisions from RHIC-BES to LHC energies. *Phys. Lett. B* **2021**, *814*, 136098.
- [55] Huovinen, P. Chemical freeze-out temperature in hydrodynamical description of Au+Au collisions at $\sqrt{s_{NN}} = 200$ GeV. *Eur. Phys. J. A* **2008**, *37*, 121–128.
- [56] Schnedermann, E.; Sollfrank, J.; Heinz, U. Thermal phenomenology of hadrons from 200A GeV S+S collisions. *Phys. Rev. C* **1993**, *48*, 2462–2475.
- [57] Abelev B.I. et al. [STAR Collaboration]. Systematic measurements of identified particle spectra in pp , d +Au, and Au+Au collisions at the STAR detector. *Phys. Rev. C* **2009**, *79*, 034909.
- [58] Abelev B.I. et al. [STAR Collaboration]. Identified particle production, azimuthal anisotropy, and interferometry measurements in Au+Au collisions at $\sqrt{s_{NN}} = 9.2$ GeV. *Phys. Rev. C* **2010**, *81*, 024911.
- [59] Tang, Z.B.; Xu, Y.C.; Ruan, L.J.; van Buren, G.; Wang, F.Q.; Xu, Z.B. Spectra and radial flow in relativistic heavy ion collisions with Tsallis statistics in a blast wave description. *Phys. Rev. C* **2009**, *79*, 051901(R).
- [60] Gutay, L.G.; Hirsch, A.S.; Pajares, C.; Scharenberg, R.P.; Srivastava, B.K. De-confinement in small systems: clustering of color sources in high multiplicity $\bar{p}p$ collisions at $\sqrt{s} = 1.8$ TeV. *Int. J. Mod. Phys. E* **2015**, *24*, 1550101.
- [61] Scharenberg, R.P.; Srivastava, B.K.; Pajares, C. Exploring the initial stage of high multiplicity proton-proton collisions by determining the initial temperature of the quark-gluon plasma. *Phys. Rev. D* **2019**, *100*, 114040.
- [62] Sahoo, P.; De, S.; Tiwari, S.K.; Sahoo, R. Energy and centrality dependent study of deconfinement phase transition in a color string percolation approach at RHIC energies. *Eur. Phys. J. A* **2018**, *54*, 136.

- [63] Wang, Q.; Liu, F.H. Excitation function of initial temperature of heavy flavor quarkonium emission source in high energy collisions. *Adv. High Energy Phys.* **2020**, *2020*, 5031494.
- [64] Wang, Q.; Liu, F.H.; Olimov, K.K. Initial-state temperature of light meson emission source from squared momentum transfer spectra in high-energy collisions. *Front. Phys. (Lausanne)* **2021**, *9*, 792039.
- [65] Waqas, M.; Liu, F.H. Initial, effective, and kinetic freeze-out temperatures from transverse momentum spectra in high energy proton(deuteron)-nucleus and nucleus-nucleus collisions. *Eur. Phys. J. Plus* **2020** *135*, 147.
- [66] Srivastava, D.K.; Chatterjee, R.; Mustafa, M.G. Initial temperature and extent of chemical equilibration of partons in relativistic collision of heavy nuclei. arXiv:1609.06496.
- [67] Soltz, R.A.; Garishvili, I.; Cheng, M.; Abelev, B.; Glenn, A.; Newby, J.; Levy, L.A.L.; Pratt, S. Constraining the initial temperature and shear viscosity in a hybrid hydrodynamic model of $\sqrt{s_{NN}} = 200$ GeV Au+Au collisions using pion spectra, elliptic flow, and femtoscopic radii. *Phys. Rev. C* **2013**, *87*, 044901.
- [68] Csanád, M. Direct photon observables from hydrodynamics and implications on the initial temperature and EoS. *PoS* **2011**, *WPCF2011*, 035.
- [69] Csanád, M. Initial temperature of the strongly interacting quark gluon plasma created at RHIC. Gribov-80 Memorial Volume, pp. 319–330 (2011) (World Scientific), arXiv:1101.1282.
- [70] Csanád, M.; Májér, I. Initial temperature and EoS of quark matter from direct photons. *Phys. Part. Nucl. Lett.* **2011**, *8*, 1013–1015.
- [71] Csanád, M.; Májér, I. Equation of state and initial temperature of quark gluon plasma at RHIC. *Cent. Eur. J. Phys.* **2012**, *10*, 850–857.
- [72] Karsch, F. Lattice QCD at finite temperature and density. *Nucl. Phys. B (Proc. Supp.)* **2000**, *83–84*, 14–23.
- [73] Gallimore, D.; Liao, J.F. A potential model study of the nucleon’s charge and mass radius. *Nucl. Phys. A* **2025**, *1055*, 123012.
- [74] Bugaev, K.A.; Ivanytskyi, A.I.; Sagun, V.V.; Grinyuk, D.E.; Savchenko, D.O.; Zinovjev, G.M.; Nikonov, E.G.; Bravina, L.V.; Zabrodin, E.E.; Blaschke, D.B.; Taranenko, A.V.; Turko, L. Hard-core radius of nucleons within the induced surface tension approach. *Universe*, **2019**, *5*, 63.
- [75] Zhu, Z.Y.; Li, A. Nucleon radius effects on neutron stars in quark mean field model. *Phys. Rev. C* **2018**, *97*, 035805.
- [76] Karsch, F.; Mehr, M.T.; Satz, H. Color screening and deconfinement for bound states of heavy quarks. *Z. Phys. C* **1988**, *37*, 617–622.
- [77] Liu, B.; Shen, P.N.; Chiang, H.C. Heavy quarkonium spectra and J/ψ dissociation in hot and dense matter. *Phys. Rev. C* **1997**, *55*, 3021–3025.
- [78] Das, T. Treatment of N-dimensional Schrödinger equation for anharmonic potential via Laplace transform. *Electron. J. Theor. Phys.* **2016**, *35*, 207–214. arXiv:1408.6139.
- [79] Das, T.; Choudhury, D.K.; Pathak, K.K. RMS and charge radii in a potential model. *Indian J. Phys.* **2016**, *90*, 1307–1312.
- [80] García, G.M. [for the ALICE Collaboration]. Quarkonium production measurements with the ALICE detector at the LHC. *J. Phys. G* **2011**, *38*, 124034.
- [81] Ma, R.R. [for the STAR Collaboration]. Measurement of J/ψ production in p+p collisions at $\sqrt{s} = 500$ GeV at STAR experiment. *Nucl. Part. Phys. Proc.* **2016**, *276–278*, 261–264.
- [82] d’Enterria, D. [for the CMS Collaboration]. High-density QCD with CMS at the LHC. *J. Phys. G* **2008**, *35*, 104039.
- [83] Kim, J.; Seo, J.; Hong, B.; Hong, J.; Kim, E.J.; Kim, Y.; Kweon, M.; Lee, S.H.; Lim, S.; Park, J. Model study on $\Upsilon(nS)$ modification in small collision systems. *Phys. Rev. C* **2023**, *107*, 054905.
- [84] Gao, Y.Q.; Liu, F.H. Comparing Tsallis and Boltzmann temperatures from relativistic heavy ion collider and large hadron collider heavy-ion data. *Indian J. Phys.* **2016**, *90*, 319–334.
- [85] Gao, L.N.; Liu, F.H.; Lacey, R.A. Excitation functions of parameters in Erlang distribution, Schwinger mechanism, and Tsallis statistics in RHIC BES program. *Eur. Phys. J. A* **2016**, *52*, 137.
- [86] Gao, L.N.; Liu, F.H. Comparing Erlang distribution and Schwinger mechanism on transverse momentum spectra in high energy collisions. *Adv. High Energy Phys.* **2016**, *2016*, 1505823.
- [87] Duan, T.T.; Yang, P.P.; Zhang, P.C.; Lao, H.L.; Liu, F.H.; Olimov, K.K. Comparing effective temperatures in standard, Tsallis, and q-dual statistics from transverse momentum spectra of identified light charged hadrons produced in gold–gold

collisions at RHIC energies. *Eur. Phys. J. Plus* **2024**, *139*, 1069.

- [88] Zhang, P.C.; Yang, P.P.; Duan, T.T.; Zhu, H.L.; Liu, F.H.; Olimov, K.K. Comparing effective temperatures in standard and Tsallis distributions from transverse momentum spectra in small collision systems. *Indian J. Phys.* **2025**, submitted. arXiv:2506.00339.
- [89] Bialas, A. Fluctuations of the string tension and transverse mass distribution. *Phys. Lett. B* **1999**, *466*, 301–304.
- [90] Florkowski, W. Schwinger tunneling and thermal character of hadron spectra. *Acta Phys. Pol. B* **2004**, *35*, 799–807.
- [91] Zardoshti, N. [ALICE Collaboration]. First direct observation of the dead-cone effect. *Nucl. Phys. A* **2021**, *1005*, 121905.
- [92] Acharya, S. [ALICE Collaboration]. Direct observation of the dead-cone effect in QCD. *Nature* **2022**, *605*, 440–446.
- [93] Thomas, R.; Kampfer, B.; Soff G. Gluon emission of heavy quarks: dead cone effect. *Acta Phys. Hung. A* **2005**, *22*, 83–91.
- [94] Herrera, D.R.; García, J.R.A.; Téllez, A.F.; Ramírez, J.E.; Pajares, C. Entropy and heat capacity of the transverse momentum distribution for pp collisions at RHIC and LHC energies. *Phys. Rev. C* **2024**, *109*, 034915.
- [95] Pirner, H.J.; Kopeliovich, B.Z.; Reygers, K. Strangeness enhancement due to string fluctuations. *Phys. Rev. D* **2020**, *101*, 114010.
- [96] Patra, R.N. [for the ALICE Collaboration]. Collective phenomena study in small systems using the bulk of particle production in high-multiplicity pp collisions at $\sqrt{s} = 13$ TeV with ALICE. *PoS* **2023**, *EPS-HEP2023*, 214.
- [97] Grosse-Oetringhaus, J.F.; Wiedemann, U.A. A decade of collectivity in small systems. *World Sci. Annu. Rev. Part. Phys.* **2025**, Invited article submitted. arXiv:2407.07484.
- [98] Song, T.; Aichelin, J.; Bratkovskaya, E. The production of primordial J/ψ in p+p and relativistic heavy-ion collisions. *Phys. Rev. C* **2017**, *96*, 014907.
- [99] Paul, B.; Mandal, M.; Roy, P.; Chattopadhyay S. Systematic study of charmonium production in pp collisions at the LHC energies. *J. Phys. G* **2015**, *42*, 065101.
- [100] Tsallis, C. Possible generalization of Boltzmann–Gibbs statistics. *J. Stat. Phys.* **1988**, *52*, 479–487.
- [101] Tsallis, C. Nonadditive entropy and nonextensive statistical mechanics—an overview after 20 years. *Braz. J. Phys.* **2009**, *39*, 337–356.
- [102] Biró, T.S.; Purcsel, G.; Urmössy, K. Non-extensive approach to quark matter. *Eur. Phys. J. A* **2009**, *40*, 325–340.
- [103] Cleymans, J.; Paradza, M.W. Statistical approaches to high energy physics: chemical and thermal freeze-outs. *Physics* **2020**, *2*, 654–664.
- [104] Parvan, A.S. Equivalence of the phenomenological Tsallis distribution to the transverse momentum distribution of q-dual statistics. *Eur. Phys. J. A* **2020**, *56*, 106.
- [105] Fischer, N.; Sjöstrand, T. Thermodynamical string fragmentation. *J. High Energ. Phys.* **2017**, *2017*, 140.
- [106] Pirner, H.J.; Kopeliovich, B.Z.; Reygers, K. Strangeness enhancement due to string fluctuations. *Phys. Rev. D* **2020**, *101*, 114010.
- [107] García, J.R.A.; Herrera, D.R.; Fierro, P.; Ramírez, J.E.; Téllez, A.F.; Pajares, C. Soft and hard scales of the transverse momentum distribution in the color string percolation model. *J. Phys. G* **2023**, *50*, 125105.
- [108] Herrera, D.R.; García, J.R.A.; Téllez, A.F.; J. E. Ramírez, J.E.; Pajares, C. Nonextensivity and temperature fluctuations of the Higgs boson production. *Phys. Rev. C* **2024**, *110*, 015205.
- [109] Boschi-Filho, H.; Braga, N.R.F.; Ferreira, C.N. Heavy quark potential at finite temperature from gauge/string duality. *Phys. Rev. D* **2006**, *74*, 086001.
- [110] Mateu, V.; Ortega, P.G.; Entem, D.R.; Fernandez, F. Calibrating the naïve Cornell model with NRQCD. *Eur. Phys. J. C* **2019**, *79*, 323.